ACADEMIC PRESS

Available online at www.sciencedirect.com

SCIENCE DIRECT®

Journal of Sound and Vibration 267 (2003) 485–496

JOURNAL OF SOUND AND VIBRATION

www.elsevier.com/locate/jsvi

On the impact noise generation due to a wheel passing over rail joints

T.X. Wu[a,*], D.J. Thompson[b]

[a] *School of Mechanical Engineering, Shanghai Jiao Tong University, Shanghai 200030, PR China*

[b] *Institute of Sound and Vibration Research, University of Southampton, Southampton SO17 1BJ, United Kingdom*

Accepted 9 May 2003

Abstract

Impacts occur when a railway wheel encounters discontinuities such as rail joints. A model is presented in which the wheel/rail impacts due to rail joints are simulated in the time domain. The impact forces are transformed into the frequency domain and converted into the form of an equivalent roughness input. Using Track–Wheel Interaction Noise Software (TWINS) and the equivalent roughness input, the impact noise radiation is predicted for different rail joints and at various train speeds. It is found that the impact noise radiation due to rail joints is related to the train speed, the joint geometry and the static wheel load. The overall impact noise level from a single joint increases with the speed V at a rate of roughly $20\log_{10}V$.

1. Introduction

The rail running surface is not perfectly smooth but contains discontinuities, the most severe of which are rail joints. The geometry of a rail joint can be characterized by the gap width and the height difference between the two sides of a gap. In addition the rail often dips near a joint. Even welded rail often has such dipped joints. These rail joints can generate large impact forces between the wheel and rail when wheels roll over a rail joint. Consequently, a transient impact noise is produced in addition to the usual rolling noise, which is more stationary in character.

A comprehensive study was carried out by Vér et al. [1] on estimating impact noise generation due to wheel and rail discontinuities. They developed simple formulae for the speed dependence of the sound power level for three types of flat rail joint (without dips). Remington [2] extended this work and estimated equivalent roughness spectra corresponding to wheel flats and rail joints to

*Corresponding author. Tel.: +86-21-6293-2640; fax: +86-21-6283-6359.

E-mail addresses: txwu@sjtu.edu.cn (T.X. Wu), djt@isvr.soton.ac.uk (D.J. Thompson).

0022-460X/$ - see front matter
doi:10.1016/S0022-460X(03)00709-0

allow comparisons of the equivalent spectrum with roughness spectra measured on wheels and rails without significant defects in terms of their noise generation capability. In a different approach, Andersson and Dahlberg [3] studied the wheel/rail impacts at a railway turnout using a finite element model with a moving vehicle.

The aim of this paper is to explore impact noise generation due to different types of rail joint using an efficient model. Equivalent relative displacement excitations between the wheel and rail are determined from the contact geometry when a wheel rolls over a rail joint. Simplified models for the wheel and track are developed and combined through a non-linear Hertzian contact stiffness, to form a wheel/rail interaction model which allows for the possibility of loss of contact between the wheel and rail. Wheel/rail impacts are simulated in the time domain using this model. Then the resulting impact forces are transformed into the frequency domain and converted into the form of equivalent roughness spectra. These are used as inputs to an established linear wheel/rail interaction model, contained in Track–Wheel Interaction Noise Software (TWINS) [4] which allows the noise radiation to be predicted for different rail joints and at various train speeds.

2. Rail joint excitation

The gap width of a rail joint may be typically 5–20 mm and the height difference between the two sides of a gap usually is in a range of 0–2 mm. Moreover, the rail often dips near a joint by several millimetres. The curve of a dipped rail near the joint can be approximated by quadratic functions. Fig. 1 shows a measured profile of a dipped joint and an approximate curve based on a quadratic function on either side of the joint. Based on the curve shown in Fig. 1, a dipped rail joint with a gap and height difference can also be described using quadratic functions.

To determine the relative displacement input between the wheel and rail, considered as elastic bodies, the trajectory of the centre of a rigid wheel rolling over the rail joint on a rigid track is required [5]. This can be determined from the fact that the wheel and the rail share a common tangent at the contact point. Fig. 2 shows a wheel rolling over a dipped rail joint with a gap and height difference. Three possible situations of wheel/rail contact are shown in Fig. 2.

In situation (a) the wheel and rail are always tangentially in contact. The position at which the wheel is in contact with both rails on the two sides of the joint can be determined according to the

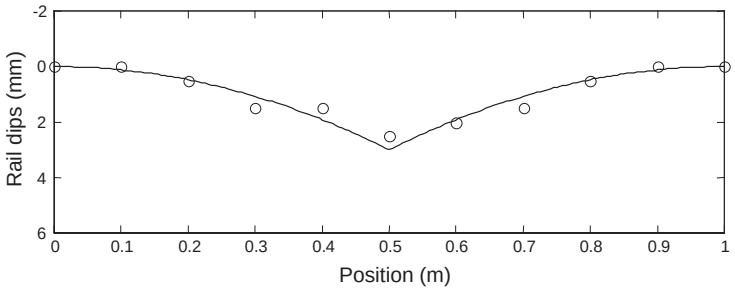

Fig. 1. Dipped rail shape at a joint. ——, from quadratic function; ○, from measurement.

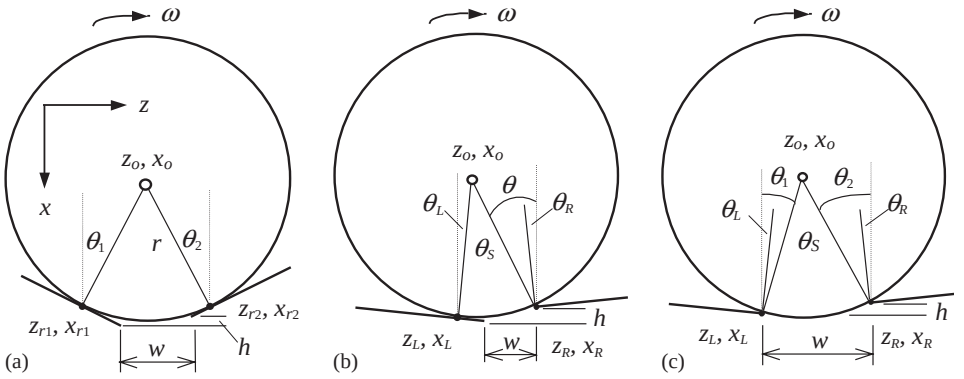

Fig. 2. Rolling contact geometry of a wheel over dipped rails at a joint.

contact geometry. Referring to Fig. 2(a), the wheel centre trajectory z_o, x_o can be given as

$$\begin{aligned} z_o &= z_{ri} + r\sin\theta_i, \\ x_o &= x_{ri} + r(1-\cos\theta_i), \quad i = 1,2, \\ \theta_i &\approx \tan\theta_i = x'_{ri}(z_{ri}), \end{aligned} \tag{1a–c}$$

where z_{ri}, x_{ri} represent the dipped rail curves, r is the wheel radius and $'$ indicates the derivative with respect to z.

In situation (b) there is a position where the wheel is tangentially in contact with the lower rail (on the left-hand side in Fig. 2(b)), but not tangentially in contact with the other rail (the higher rail on the right-hand side). From this position the wheel will pivot about the contact point with the higher rail until the wheel is tangentially in contact with the rail. The wheel centre trajectory in this transitional stage can be calculated using the following formula:

$$\begin{aligned} z_o &= z_R - r\sin\theta, \\ x_o &= x_R + r(1-\cos\theta), \end{aligned} \tag{2a, b}$$

where $\theta_S - \theta_L \geqslant \theta \geqslant \theta_R$ and θ_S, θ_L and θ_R can be determined according to the wheel radius and the rail joint geometry, see Fig. 2(b).

Situation (c) is for a wide gap at the joint which rarely appears in practice, for example, a gap greater than 20 mm at a 5 mm deep dipped joint without height difference. The wheel centre trajectory in the stage of non-tangential contact can be given as follows, see Fig. 2(c):

$$\begin{aligned} z_o &= z_L + r\sin\theta_1 \\ x_o &= x_L + r(1-\cos\theta_1) \end{aligned} \quad \text{for } \theta_L \leqslant \theta_1 \leqslant \frac{\theta_S}{2} - \delta, \tag{3a, b}$$

$$\begin{aligned} z_o &= z_R - r\sin\theta_2 \\ x_o &= x_R + r(1-\cos\theta_2) \end{aligned} \quad \text{for } \frac{\theta_S}{2} + \delta \geqslant \theta_2 \geqslant \theta_R, \tag{3c, d}$$

where $\delta = \tan^{-1}(h/w)$, h is the height difference and w is the gap width.

As neither the track nor the wheel are rigid, the actual motion of the wheel centre is much more complicated than that described in Eqs. (1)–(3). Nevertheless, Eqs. (1)–(3) can be used as the

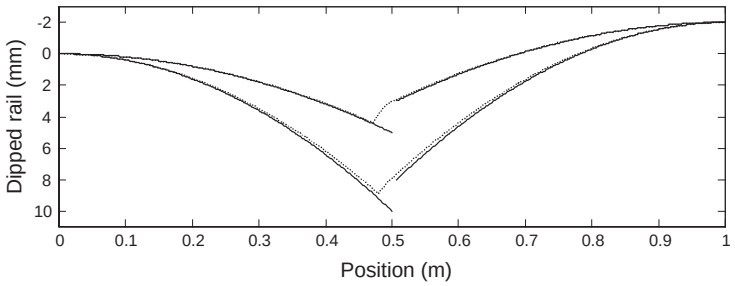

Fig. 3. Wheel centre trajectory for a wheel rolling over a dipped rail joint. ——, dipped rail shape; · · · · ·, wheel centre trajectory. Upper curves are for a 5 mm dip at the joint, bottom curves for a 10 mm dip at the joint.

relative displacement excitation between a flexible track and wheel in the wheel/rail interaction model. In each case in Fig. 2 the left-hand side is lower than the right-hand side. This represents a so-called 'step-up' joint. For a 'step-down' joint the above expressions are still valid but for the opposite direction of the longitudinal position of the wheel centre, z_o.

Fig. 3 shows two examples of the wheel centre trajectory calculations. In both cases the joint gap $w = 7$ mm and the step-up size $h = 2$ mm. The joint with 10 mm dip corresponds to situation (a), and that with 5 mm dip to situation (b). The calculated wheel centre trajectories are very close to the dipped rail curves, especially for the rail with the smaller dip, where a step-up transition from the lower rail to the higher one is rather noticeable in the wheel centre trajectory. It is found that the gap width of a joint is a less important factor affecting the wheel centre trajectory, compared with the step-up size, provided that the gap width is not large, e.g., $w \leqslant 20$ mm.

3. Simulation of wheel/rail impact

A relative displacement excitation model is used to calculate the vertical wheel/rail interaction [6]. In such a model the wheel remains stationary on the rail and the wheel centre trajectory x_o described in Eqs. (1)–(3) is effectively moved at the train speed between the wheel and rail as an excitation [5]. The wheel/track interaction model is shown schematically in Fig. 4.

The vehicle above the suspension is simplified to a static load W. The track model is composed of a pair of semi-infinite Timoshenko beams on a continuous spring–mass–spring foundation representing the rail pads, sleepers and ballast respectively. The reason for using semi-infinite beams as an approximation of jointed rails is that the bending stiffness of the rail at a joint is dramatically reduced.

As both the track and the wheel are assumed to be linear, they can be represented by equivalent systems that have the same frequency response functions. The track is approximated by a system with the following frequency response function:

$$H_r(s) = \frac{X(s)}{F(s)} = \frac{(b_1 s^3 + b_2 s^2 + b_3 s + b_4)}{(s^4 + a_1 s^3 + a_2 s^2 + a_3 s + a_4)}, \tag{4}$$

where $X(s)$ and $F(s)$ are the Laplace transforms of the displacement (output) and the force (input) at the contact position respectively. Constant coefficients a_i and b_i are determined by minimizing

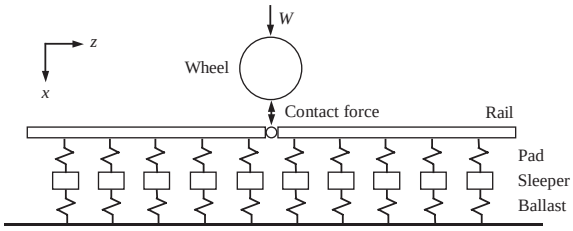

Fig. 4. Wheel/track interaction model at a joint.

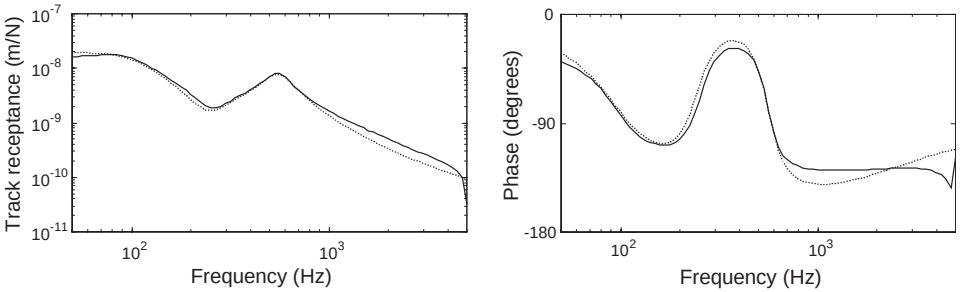

Fig. 5. Track receptance at contact point at a rail joint. ——, from full model; · · · · ·, from approximate model.

the differences between $H_r(\mathrm{i}\omega)$ and the point receptance of the full track model in the frequency region of interest. This model was first developed by Wu and Thompson [7] for an infinite track. Good agreement can be seen in Fig. 5 between the approximate and full track models in terms of the point receptance. The track parameters used here are for UIC 60 rail (60 kg/m) on monobloc concrete sleepers. The sleeper mass is 270 kg/m. The rail pad stiffness is 583 MN/m^2 and the ballast stiffness is 83.3 MN/m^2. Damping is added to the pad and ballast via loss factors which are 0.25 and 1.0 respectively.

The wheel is approximated by its unsprung mass, M, together with a damped spring, K and c, giving the following transfer function (receptance):

$$H_w(\omega) = -(K - M\omega^2 + \mathrm{i}\omega c)/M\omega^2(K + \mathrm{i}\omega c), \tag{5}$$

where $M = 600$ kg, $K = 4590$ MN/m and $c = 1660$ N s/m. Obviously the high frequency modes of a wheel are not present in this model, but they can be well compensated using a hybrid model of wheel/rail interaction in the frequency domain [5]. This is discussed in Section 4.

Coupling the equivalent track and wheel models given by Eqs. (4)–(5) through a Hertzian contact force, the wheel/rail interaction can be expressed in the time domain using a state-space form. The non-linear Hertzian contact force is given as

$$f = \begin{cases} C_H(x_w - x_r - x_o)^{3/2}, & x_w - x_r - x_o > 0, \\ 0, & x_w - x_r - x_o \leqslant 0, \end{cases} \tag{6}$$

where C_H is the Hertzian constant and $C_H = 9.37 \times 10^{10}$ N/m$^{3/2}$, x_w and x_r are the displacement of the wheel and rail respectively and x_o is the relative displacement excitation due to the wheel

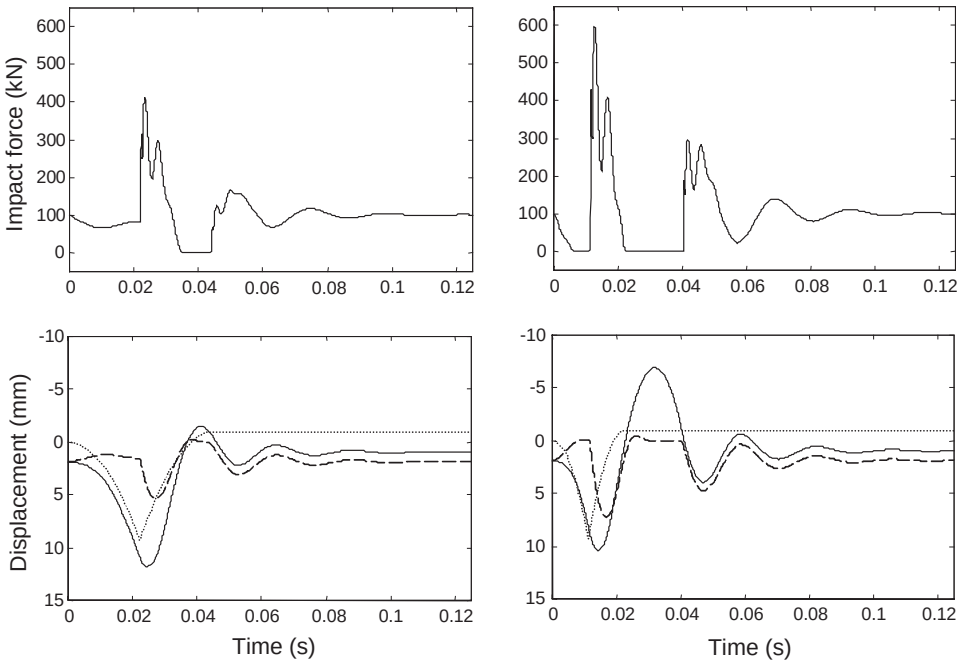

Fig. 6. Wheel/rail impact at a dipped rail joint with a gap $w = 7$ mm and a step-up $h = 1$ mm and under a static load $W = 100$ kN. Left: at 80 km/h. Right: at 160 km/h. Upper: impact force. Lower: ——, wheel displacement; - - -, rail displacement; · · · · ·, wheel centre trajectory (relative displacement excitation).

rolling over a rail joint, described for example in Eqs. (1)–(3) for the different types of joint. Here x_o is a function of time and thus becomes dependent upon the train speed.

Simulations of wheel/rail impact are carried out for different types of rail joint and at various train speeds. Fig. 6 shows the wheel/rail impact process for a dipped rail joint with a gap width $w = 7$ mm and height difference $h = 1$ mm (step-up). The dipped rail sections are chosen as 0.5 m long on each side of the joint and symmetrical about the joint as in Fig. 1, with the largest dip being 10 mm at the joint. A static force $W = 100$ kN is applied to the wheel to represent the vehicle load. Impact occurs when the wheel rolls over the joint from one rail onto the other, or after loss of contact between the wheel and rail, where the inertia force of the wheel is greater than the static load. During impact the contact force rises dramatically and the ratio of the peak to the static load reaches 4 and 6 at speeds 80 and 160 km/h respectively. If the train speed is low, loss of contact may not appear, but impact still occurs with a smaller peak.

The results in Fig. 6 illustrate that the impact force caused by rail joints is related to the train speed. The ratio of the peak to the static load at different speeds is presented in Fig. 7 for different types of rail joint with a 7 mm gap. In general, the maximum impact force increases as the speed goes up. For the rail with 5 mm dip, the peak becomes larger and larger as the step-up size increases from 0 to 3 mm, whilst the rate of increase is small for the 5 mm step-down joints. On the other hand, for the 10 mm dipped rail, it shows only slight changes in both step-up and step-down cases. This indicates that the height difference of a rail joint affects the wheel/rail impact more significantly for the lightly dipped rail than for the deeply dipped rail.

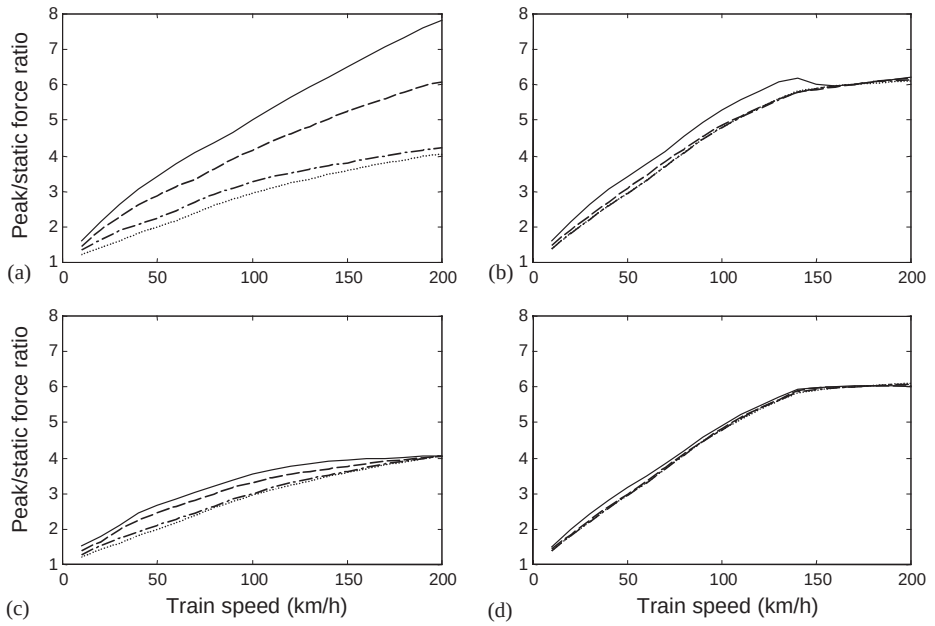

Fig. 7. Ratio of the maximum impact force to the static load: (a) for step-up joints with 5 mm dip, (b) for step-up joints with 10 mm dip, (c) for step-down joints with 5 mm dip, (d) for step-down joints with 10 mm dip. · · · · · , height difference $h = 0$; - · · · -, $h = 1$ mm; - - -, $h = 2$ mm; ——, $h = 3$ mm.

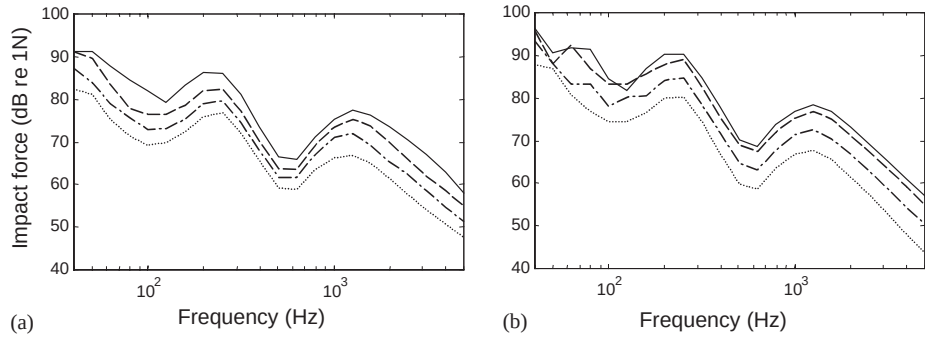

Fig. 8. Impact force spectra in one-third octave bands due to a wheel passing over a rail joint with 7 mm gap and 1 mm height difference at various speeds: (a) from a step-up joint with 5 mm dip, (b) from a step-up joint with 10 mm dip. · · · · · , 50 km/h; - · · · -, 80 km/h; - - -, 120 km/h; ——, 200 km/h.

As the wheel and the track are assumed to be linear, their responses to the excitation can be calculated in the frequency domain. Fig. 8 shows the frequency components of the impact force (during 0.125 s) in one-third octave bands due to different rail joints at various speeds. The spectra all have a similar shape and increase with increasing train speed. The local peaks at about 240 Hz and the local troughs at about 550 Hz in the force spectra correspond to the trough at 240 Hz and the peak at 550 Hz in the point receptance of the track (refer to Fig. 5).

4. Wheel and track radiation

TWINS models [4] for predicting rolling noise due to random roughness are normally used in the frequency domain with a linear interaction model. For a roughness excitation between the wheel and rail, $R(\omega)$ at angular frequency ω, and considering only interaction in the vertical direction, the interaction force $F(\omega)$ is given by

$$F(\omega) = -\frac{R(\omega)}{[\alpha^W(\omega) + \alpha^C(\omega) + \alpha^R(\omega)]}, \tag{7}$$

where α^W, α^C and α^R are the receptances of the wheel, contact spring and rail respectively.

In order to use TWINS to predict impact noise due to rail joints, the impact force spectrum must be converted back to 'an equivalent roughness spectrum', which is the roughness (relative displacement) input that would produce the same force spectrum if the contact spring were linear and there were no loss of contact between the wheel and rail. This is done by using Eq. (7) in reverse:

$$R_{eq}(\omega) = -F(\omega)(\alpha^W(\omega) + \alpha^C(\omega) + \alpha^R(\omega)), \tag{8}$$

where $F(\omega)$ is the impact force spectrum and α^C, the receptance of the contact spring, is from a linear contact spring equivalent to the non-linear Hertzian contact stiffness. The equivalent roughness spectra corresponding to the impact forces due to a wheel passing over rail joints then can be used as inputs into TWINS to predict noise radiation from the wheel and track.

It is known from studies of rolling noise that the wheel modes containing a significant radial component of motion at the contact zone dominate the noise radiation of the wheel/rail system in the frequency region above about 2 kHz [8]. Although the force $F(\omega)$ is calculated from the simplified wheel model, it has been found in Ref. [5] that the high frequency modes of the wheel can be taken into account quite precisely by using the equivalent roughness input, even though these modes are not present in the simplified model and thus excluded from the simulations of the wheel/rail impact in the time domain.

In TWINS, the wheel is represented by its full modal basis up to 6 kHz, and the track is modelled by an infinite Timoshenko beam continuously supported on layers of damped springs and mass. Wheel/rail interaction is included in both vertical and lateral directions, the excitation being in the vertical direction. The results from TWINS are corrected to convert them to the situation modelled, in which the rail is semi-infinite with a pin joint at the excitation point.

Fig. 9 shows the equivalent roughness spectra corresponding to the impact force spectra in Fig. 8 and the predicted overall sound power radiated by one wheel and the associated track vibration. The sound power represents the radiation emitted during 0.125 s. The equivalent roughness spectrum can be seen to increase with increasing speed and to reduce with frequency. The noise radiation increases at all frequencies as the speed increases. For step-down joints the equivalent roughness and the radiation are similar and thus are not shown.

Fig. 10 presents a summary of the variation of the overall A-weighted sound power level with train speed for different rail joints. All the curves show that the noise radiation generally increases with increasing speed. For the lightly dipped rail with a step-up joint (5 mm dip at the joint), the predicted noise level steadily increases at a rate of approximately $20 \log_{10} V$, where V is the train speed. The rate of increase for a step-down joint is not as high as for a step-up joint. For the

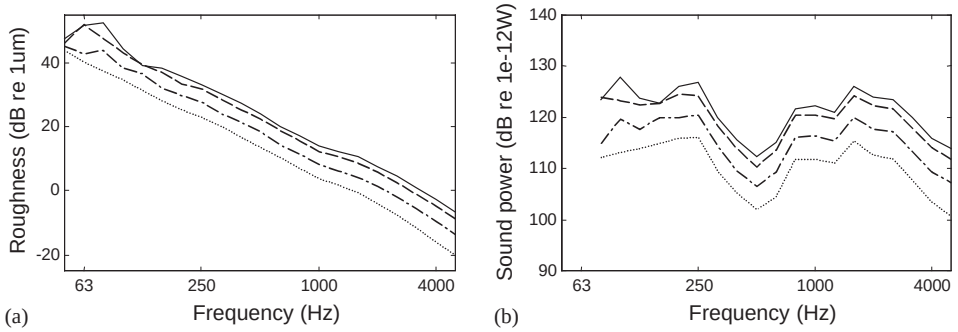

Fig. 9. Equivalent one-third octave roughness spectra and sound power levels due to a wheel passing over a rail joint with 7 mm gap, 1 mm step-up and 10 mm dip at various speeds. · · · · ·, 50 km/h; - · - · -, 80 km/h; - - -, 120 km/h; ——, 200 km/h.

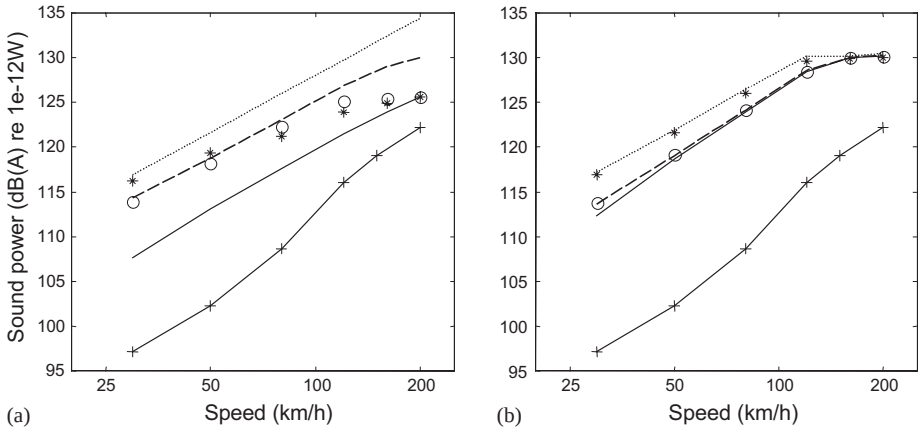

Fig. 10. A-weighted sound power radiated by one wheel and the associated track vibration during 0.125 s due to a wheel passing over different rail joints with 7 mm gap and 5 or 10 mm dip. (a) for 5 mm dip, (b) for 10 mm dip. · · · · ·, 2 mm step-up; - - -, 1 mm step-up; ——, no height difference; ∗, 2 mm step-down; ○, 1 mm step-down; +—+, rolling noise due to roughness (tread-braked wheel and smooth rail).

lightly dipped rail, the noise radiation increases significantly by up to 8 dB when the step-up size increases from 0 to 2 mm, whereas for the more deeply dipped rail (10 mm dip at the joint), it remains almost unchanged when the step-up size increases from 0 to 1 mm, and increases only at most 3 dB from 1 mm to 2 mm. Moreover, the results for the 10 mm dip are similar for both step-up and step-down joints. This indicates that, in this case, the shape of the dipped rail at the joint affects the noise radiation more significantly, whereas for the lightly dipped rail, it is the height difference between the two sides of a joint that affects the noise radiation more significantly. Also shown is the predicted rolling noise level due to typical roughness on tread-braked wheels and smooth rail, which increases at a rate of approximately $30 \log_{10} V$.

Fig. 11 shows the overall A-weighted sound power level plotted against train speed for dipped rails with a 1 mm step-up joint at two values of wheel load, 50 and 100 kN. This corresponds to the difference between typical passenger vehicles (50 kN) and loaded freight vehicles (100 kN).

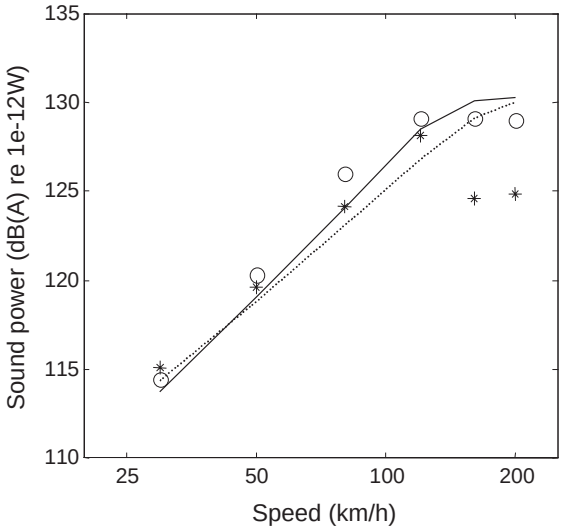

Fig. 11. A-weighted sound power radiated by one wheel and the associated track vibration during 0.125 s due to a wheel passing over a 1 mm step-up joint with 7 mm gap and at two values of wheel load. ——, 10 mm dip and 100 kN load; ○, 10 mm dip but 50 kN load; · · · · ·, 5 mm dip and 100 kN load; ∗, 5 mm dip but 50 kN load.

Greater loss of contact between the wheel and rail occurs for 50 kN than for 100 kN but the peak impact force is lower for the former than for the latter. In addition, the corresponding TWINS calculations include the effect of the change in the contact stiffness. The final effects on the noise radiation are therefore a combination of all the above factors. From Fig. 11 the noise level can be seen to increase slightly at the speeds up to 120 km/h as the wheel load is reduced, and to reduce at high speeds by about 5 dB for the lightly dipped rail joint. The effects of the static load on impact noise generation are thus rather complicated.

The noise level in Fig. 10 is based on an averaging time of 0.125 s. This is the averaging time of a sound level meter in the 'fast' setting, and gives an indication of short-term perception. In comparing impact noise levels with rolling noise levels, the averaging time must to be adjusted to the time between two rail joints, normally 18 m apart. As this time reduces with increasing speed, it is found that the average noise over a period of 18 m travel due to impacts increases at a rate of $30\log_{10}V$, similar to rolling noise. The equivalent noise from dipped rail joints is found to be 0–10 dB higher than that from rolling noise, as shown in Fig. 12.

5. Conclusions

Impact noise generation due to a wheel passing over dipped rail joints has been studied using an efficient theoretical model for different rail joints and at various train speeds. The wheel/rail impact and the consequent impact noise radiation from the wheel and track are found to be related to the train speed, the geometry of the rail joint and the static wheel load. As the train speed increases, the overall impact noise level from a single joint increases with train speed V at a rate of roughly $20\log_{10}V$. This differs from rolling noise due to roughness excitation which

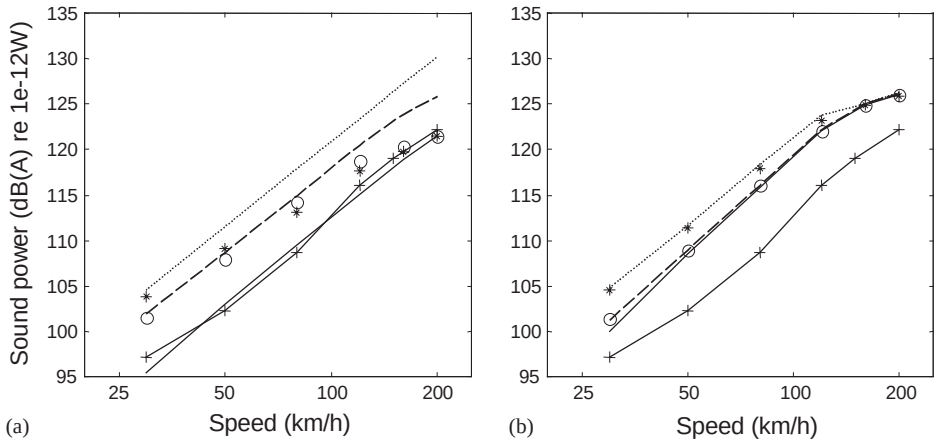

Fig. 12. Equivalent A-weighted sound power radiated by one wheel and the associated track vibration due to wheel/rail impact averaged over a period of 18 m travel, key as for Fig. 10.

generally increases at $30\log_{10}V$. However for a jointed track with regularly spaced joints, the contribution of the impact noise to the equivalent continuous level will also increase at $30\log_{10}V$. A large difference in height between the two sides of a step-up joint may generate higher level impact noise for a lightly dipped rail than for a deeply dipped rail. For a lightly dipped rail, a step-down joint usually generates less noise than a step-up joint, whilst for a deeply dipped rail, the noise levels are the same for both types of joint. The effects of the static load on impact noise generation are complicated. Under smaller static load, greater loss of contact between the wheel and rail may occur and the noise level may increase at lower speeds, but at higher speeds it reduces.

Acknowledgements

The work described was carried out while the first author was at ISVR, and has been performed within the 'Non-linear Effects at the Wheel/rail Interface and their Influence on Noise Generation' project, funded by Engineering and Physical Sciences Research Council of the United Kingdom (EPSRC), grant GR/M82455. The authors are grateful to J.W. Edwards of Infraco BCV (formerly London Underground) for supplying dimensions of typical rail joints.

References

[1] I.L. Vér, C.S. Ventres, M.M. Myles, Wheel/rail noise—part III: impact noise generation by wheel and rail discontinuities, *Journal of Sound and Vibration* 46 (1976) 395–417.

[2] P.J. Remington, Wheel/rail squeal and impact noise: what do we know? What don't we know? Where do we go from here?, *Journal of Sound and Vibration* 116 (1987) 339–353.

[3] C. Andersson, T. Dahlberg, Wheel/rail impacts at a railway turnout crossing, *Proceedings of the Institution of Mechanical Engineers F* 212 (1998) 123–134.

[4] D.J. Thompson, M.H.A. Janssens, TWINS: track–wheel interaction noise software, theoretical manual, version 2.4, TNO report TPD-HAG-RPT-93-0214, TNO Institute of Applied Physics, 1997.
[5] T.X. Wu, D.J. Thompson, A hybrid model for the noise generation due to railway wheel flats, *Journal of Sound and Vibration* 251 (2002) 115–139.
[6] S.L. Grassie, R.W. Gregory, D. Harrison, K.L. Johnson, The dynamic response of railway track to high frequency vertical excitation, *Journal of Mechanical Engineering Science* 24 (1982) 77–90.
[7] T.X. Wu, D.J. Thompson, Theoretical investigation of wheel/rail non-linear interaction due to roughness excitation, *Vehicle System Dynamics* 34 (2000) 261–282.
[8] D.J. Thompson, C.J.C. Jones, A review of the modelling of wheel/rail noise generation, *Journal of Sound and Vibration* 231 (2000) 519–536.